PERGAMON

International Journal of Heat and Mass Transfer 43 (2000) 3417–3432

International Journal of HEAT and MASS TRANSFER

www.elsevier.com/locate/ijhmt

Volumetric heat transfer coefficients in solid–fluid porous media: closure problem, thermal analysis and model improvement with fluid flow

H.Y. Zhang, X.Y. Huang*

School of Mechanical and Production Engineering, Nanyang Technological University, Nanyang Avenue, Singapore 639798, Singapore

Received 14 February 1999; received in revised form 28 October 1999

Abstract

This paper presents a detailed investigation on the volumetric transfer coefficient (VHTC) model in solid–fluid porous media based on the volume averaging method (VAM). The VHTC is obtained by solving the closure problem with the control-volume finite difference method. A thermal analysis is conducted to illustrate the thermal nature of the VHTC, based on which, an improved VHTC model has been proposed by taking into account the effects of the thermal entrance and the non-uniformity of the velocity field. With this model, the applicability of the VAM has been extended to large Peclet number laminar regime for convection heat transfer in porous media characterized by straight ducts.

1. Introduction

In engineering applications, such as thermal energy storage units and cooling of electronics components, consolidated porous matrices with high thermal conductivity have been used to enhance the overall thermal performance. The heat transfer mechanisms in such porous media involve not only heat transport in each single phase, but also the heat exchange between the matrices and the transport fluids. Thus, a theoretical prediction of the heat transfer coefficient is of great practical concern.

In the volume averaging method (VAM), a closure problem in term of dimensionless closure variable ψ has been developed to evaluate the volumetric heat transfer coefficient (VHTC) [1,2]. Being different from the conventional temperature quantity, the closure variable ψ (which is denoted as ψ_f if in the fluid and ψ_s if in the solid) is mathematically defined as the first order coefficient in the local expansion of the phasic temperature difference. Such a closure problem is featured by the jump condition at the solid–fluid interface and the periodic boundary conditions. Its solution is dependent on the geometry of the microstructure, the thermophysical properties of the constituents and the average velocity field. The analytical solution of the closure problem and the VHTC for a circular tube case was given in [3]. Quintard and Whitaker [2] discussed the development of the closure problem in a mathematical manner. They also presented a numerical solution for the two-dimensional unit cell in granular porous media. However, the thermal nature of the closure problem and the VHTC were not discussed in their study. In the work by Grangeot et al. [4], the VHTC is evaluated by fitting the measured temperature profiles with a system of phenomenological energy

* Corresponding author.
E-mail address: mxhuang@ntu.edu.sg (X.Y. Huang).

0017-9310/00/$ - see front matter
PII: S0017-9310(99)00370-1

Nomenclature

a, b	geometrical quantities, Fig. 7
A_{fs}	interfacial area
A_W, A_E	coefficients in the discretized equation
$\boldsymbol{b}_{ff}$, $\boldsymbol{b}_{fs}$, $\boldsymbol{b}_{sf}$, $\boldsymbol{b}_{ss}$	vector closure variables related to thermal conductivities
$(\rho c)_f$	heat capacity of the fluid
c_0	constant
c_{ff}, c_{fs}	source terms in the closure problem, Eqs. (5a) and (5b)
$f(x)$	modification function, Eq. (21)
H, H_f	dimensionless volumetric heat transfer coefficients, Eqs. (2a)–(2c)
$H(x)$	modified heat transfer coefficient model, Eq. (20)
k	thermal conductivity
$\mathbf{K}_{eff}$	effective thermal conductivity tensor
$K_{ff,\,zz}$, $K_{fs,\,zz}$, $K_{sf,\,zz}$, $K_{ss,\,zz}$	zz components of the thermal conductivity tensors
$\boldsymbol{l}$	lattice vector
l, L	characteristic microscopic length scale and macroscopic length scale
$\boldsymbol{n}_{fs}$	normal vector from the fluid to solid
Nu_x	local Nusselt number for a circular tube
Pe_l	$\langle u\rangle^f l_f/\alpha_f$, microscopic Peclet number
Pe_L	$\langle u\rangle^f L/\alpha_f$, macroscopic Peclet number
q	heat flux through the interface
$\boldsymbol{r}$	position vector
r	cylindrical coordinate
r_0, r_1	radii of the circular unit cells, Fig. 1
s	solid phase
Su	source term in numerical procedure
T	temperature
$\langle T\rangle$	$\varepsilon_f\langle T_f\rangle^f+\varepsilon_s\langle T_s\rangle^s$, spatial average temperature
T_{fs}	temperature at the interface
$\langle T_f\rangle^f$, $\langle T_s\rangle^s$	intrinsic averages of the fluid and solid temperature, respectively
$\boldsymbol{u}$	velocity vector
$\langle\boldsymbol{u}\rangle^f$	intrinsic average of the vector velocity
u	vector scalar; velocity component in x direction
V	volume
x, y, z	rectangular coordinates

Greek symbols

Ω	phasic domain
α	thermal diffusivity
β	aspect ratio
ε_f, ε_s	volume fraction of the fluid and the solid, respectively
φ	general variable used in numerical procedure
γ	phase-identifying function, Eq. (4a)
κ	k_s/k_f, solid to liquid conductivity ratio
σ	phase-identifying function, Eq. (4b)
ψ	heat exchange related closure variable
ψ_I	unified closure variable

Subscripts

+	RHS of a control volume face
−	LHS of a control volume face
f	fluid phase
s	solid phase

Superscripts

f	intrinsic average in the fluid
s	intrinsic average in the solid
′	deviation quantity

equations. The VHTC obtained in this way differed from their numerical result. As to the availability of the VHTC for thermal energy transport in porous media, most studies are limited to pure heat conduction problems [2,4,5]. For convection heat transfer in porous media, the application of the VAM has been reviewed in the monograph [6]. In a recent work [7], it was found that a full-version of the VAM formulation with the constant VHTC model seemed *unable* to predict large Peclet number convection heat transfer with enough accuracy. It is believed that a thorough investigation of the VHTC is of both theoretical and practical significance.

In this paper, the VHTC model in solid–fluid porous media is investigated in detail. Consolidated unit cells are used throughout the study. First, the numerical solution of the closure problem is described and the VHTC results for different unit cells are given. Phase-identifying functions are introduced to denote the geometric domains and to unify the closure equations of the two phases. A thermal analysis of the VHTC is then presented and illustrated by examining the analogous thermal problems. This thermal analysis also serves as a theoretical basis on which the VHTC model can be modified according to the analogous heat transfer mechanism occurring at the microscopic

level. One example is shown for convection heat transfer in porous media by incorporating the heat transfer theory for a single circular tube in an improved model.

2. Closure problem and solution procedure

2.1. Closure problem and VHTC

In the VAM, the closure problem in term of ψ variable for solid–fluid porous media is given as [1,2]

$$\left[(\rho c)_{\mathrm{f}}\langle \boldsymbol{u}\rangle^{\mathrm{f}}\cdot\nabla\psi_{\mathrm{f}}\right] = \nabla\cdot\left(k_{\mathrm{f}}\nabla\psi_{\mathrm{f}}\right) - \frac{k_{\mathrm{f}}}{V_{\mathrm{f}}}\int \boldsymbol{n}_{\mathrm{fs}}\cdot\nabla\psi_{\mathrm{f}}\,\mathrm{d}A_{\mathrm{fs}} \tag{1a}$$

$$0 = \nabla\cdot\left(k_{\mathrm{s}}\nabla\psi_{\mathrm{s}}\right) - \frac{k_{\mathrm{s}}}{V_{\mathrm{s}}}\int \boldsymbol{n}_{\mathrm{sf}}\cdot\nabla\psi_{\mathrm{s}}\,\mathrm{d}A_{\mathrm{fs}} \tag{1b}$$

$$\psi_{\mathrm{f}} = \psi_{\mathrm{s}} + 1, \tag{1c}$$

$$\boldsymbol{n}_{\mathrm{fs}}\cdot k_{\mathrm{f}}\nabla\psi_{\mathrm{f}} = \boldsymbol{n}_{\mathrm{fs}}\cdot k_{\mathrm{s}}\nabla\psi_{\mathrm{s}} \quad \text{at } A_{\mathrm{fs}} \tag{1d}$$

and periodic boundary conditions are:

$$\psi_{\mathrm{f}}(\boldsymbol{r}+\boldsymbol{l}) = \psi_{\mathrm{f}}(\boldsymbol{r}) \tag{1e}$$

$$\psi_{\mathrm{s}}(\boldsymbol{r}+\boldsymbol{l}) = \psi_{\mathrm{s}}(\boldsymbol{r}). \tag{1f}$$

As the closure variables ψ_{f} and ψ_{s} are deviation quantities, their intrinsic averages are imposed to be zero. Here the subscripts f and s represent the fluid and the solid, respectively. Eq. (1c) shows a jump condition at the solid–fluid interface. In the above closure problem, the fluid flow has been assumed incompressible and laminar. The porous medium is homogeneous and the thermophysical properties are assumed to be constants over a representative unit cell, or at the microscopic level. Given the geometry of the unit cell, the two phases and the average velocity $\langle u\rangle^{\mathrm{f}}$, the closure problem is solvable. From the ψ field one can obtain the VHTC by the following formula

$$H = \frac{l^2}{V}\int \boldsymbol{n}_{\mathrm{fs}}\cdot\nabla\psi_{\mathrm{f}}\,\mathrm{d}A_{\mathrm{fs}}. \tag{2a}$$

For the time being we pay our attention to a class of consolidated porous media with heat transfer enhancement bearing in mind. In the consolidated porous medium system, the solid matrix, acting as a bridge, conducts heat from the source and then transfers it to the cooling fluid or thermal storage units. Fig. 1 shows three kinds of consolidated unit cells used in this study:

RR: rectangular unit cell with a rectangular fluid domain;
RC: rectangular unit cell with a circular fluid domain;
CC: idealized circular unit cell with a circular fluid domain.

It is convenient to have the VHTC based on the length scale of the fluid domain:

$$H_{\mathrm{f}} = \frac{l_{\mathrm{f}}^2}{V_{\mathrm{f}}}\int \boldsymbol{n}_{\mathrm{fs}}\cdot\nabla\psi_{\mathrm{f}}\,\mathrm{d}A_{\mathrm{fs}} \quad \text{for case RR,} \tag{2b}$$

$$H_{\mathrm{f}} = \frac{r_0^2}{V_{\mathrm{f}}}\int \boldsymbol{n}_{\mathrm{fs}}\cdot\nabla\psi_{\mathrm{f}}\,\mathrm{d}A_{\mathrm{fs}} \quad \text{for cases RC and CC.} \tag{2c}$$

The relationship of H and H_{f} is

$$H = \varepsilon_{\mathrm{f}}(l/l_{\mathrm{f}})^2 H_{\mathrm{f}} = 4H_{\mathrm{f}} \quad \text{for case RR,}$$
$$H = \varepsilon_{\mathrm{f}}(l/r_0)^2 H_{\mathrm{f}} = \pi H_{\mathrm{f}} \quad \text{for cases RC and CC,}$$

where the fluid volume fraction $\varepsilon_{\mathrm{f}} = (l_{\mathrm{f}}/l_{\mathrm{s}})^2$ and the geometrical relation $\pi r_0^2 = 4l_{\mathrm{f}}^2$ has been used. For case CC, an analytical solution for the heat transfer coefficient has been given in [3], which can be rearranged as

$$H_{\mathrm{f}} = \frac{8}{1 + \left(-2\ln\varepsilon_{\mathrm{f}} - 2\varepsilon_{\mathrm{s}} - \varepsilon_{\mathrm{s}}^2\right)/\varepsilon_{\mathrm{s}}^2\kappa}. \tag{3}$$

Here the sum in the brackets is always positive in spite of the three negative terms in form.

In the presence of a tortuous flow, the VHTC is correlated with the average velocity $\langle u\rangle^{\mathrm{f}}$. For cases of fluid flow in straight ducts or pure heat conduction problems, the convection term in Eq. (1a) vanishes and the periodic boundary conditions, Eqs. (1e) and (1f), reduce to zero-gradient boundary conditions for symmetric unit cells [2] (we use symmetric unit cells throughout this study). To obtain the VHTC, the closure problem in term of ψ need to be solved by numerical techniques since analytical solutions are not available except for very few cases. In the present study, the numerical discretization is based on the control-volume finite difference method developed by Patankar [8].

2.2. Solution procedure

In solving the closure problem, phase-identifying functions are introduced to denote the domains of different phases. The basic phase-identifying function is

$$\gamma = \begin{cases} 0 & \text{at } \Omega_{\mathrm{f}} \\ 1 & \text{at } \Omega_{\mathrm{s}} \end{cases} \tag{4a}$$

The conductivity related phase-identifying function is

$$\sigma = \begin{cases} k_f & \text{at } \Omega_f \\ k_s & \text{at } \Omega_s \end{cases}. \tag{4b}$$

With the above phase-identifying functions, we can unify Eqs. (1a) and (1b) into the following form

$$(1-\gamma)(\rho c)_f \langle \boldsymbol{u} \rangle^f \cdot \nabla \psi_I = \nabla \cdot \left(\sigma \nabla \psi_I\right) - \gamma c_{sf} - (1-\gamma) c_{ff} \tag{5a}$$

where the unified variable ψ_I is given by

$$\psi_I = \begin{cases} \psi_f & \text{at } \Omega_f \\ \psi_s & \text{at } \Omega_s \end{cases}, \tag{5b}$$

and c_{sf} and c_{ff} represent the interfacial integrals of Eqs. (1a) and (1b), taking the form

$$c_{ff} = \frac{k_f}{V_f} \int \boldsymbol{n}_{fs} \cdot \nabla \psi_f \, \mathrm{d}A_{fs} \tag{5c}$$

$$c_{sf} = -\frac{k_s \varepsilon_f}{\varepsilon_s} c_{ff}. \tag{5d}$$

For the sake of convenience, rectangular grid systems with equally spaced steps are employed for two- and three-dimensional unit cells. The grid blocks for cases RR and RC are shown schematically in Fig. 2, with the shadowed domains representing the solid phase. Each grid block corresponds to one control volume. The solid–fluid interface is defined at the locations of the control volume faces.

In cases such as fluid flow through straight ducts or pure conduction problems, the convective term is zero and Eq. (5a) can be discretized in the standard form. For example, considering the control volume P in the one-dimensional grid blocks shown in Fig. 2(c), the discretized equation for Eq. (5a) without the convective term takes the form

$$A_p \varphi_p = A_W \varphi_W + A_E \varphi_E + S u_P, \tag{6a}$$

where Su_P is referred to as the source term. The coef-

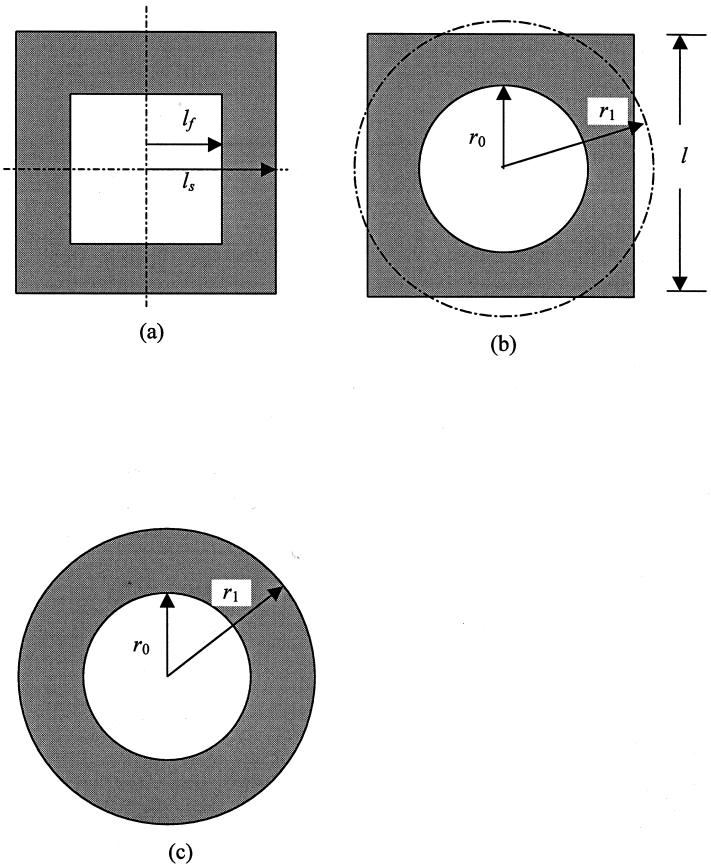

Fig. 1. Two-dimensional unit cell: (a) case CC; (b) case RC; (c) case RR. The shadowed and the hollow domains represent the solid and the fluid, respectively.

ficients A_W and A_E are given in harmonic mean,

$$A_W = \frac{1}{x_{w-}/\sigma_{w-} + x_{w+}/\sigma_{w+}}, \tag{6b}$$

$$A_E = \frac{1}{x_{e-}/\sigma_{e-} + x_{e+}/\sigma_{e+}}, \tag{6c}$$

where the subscript '−' stands for values taken on the left side of the control volume face and '+' for values on the right side, as shown in the grid system Fig. 2(c), and

$$A_P = A_W + A_E. \tag{6d}$$

With the phase-identifying functions, the source term of the control volume next to the interface, P, can be written as

$$Su_P = Su_P + A_E(\gamma_+ - \gamma_-), \tag{6e}$$

where the term containing $(\gamma_+ - \gamma_-)$ stands for the additional source term due to the jump condition in Eq. (1c). The difference $(\gamma_+ - \gamma_-)$ denotes the unit normal vector $\boldsymbol{n}_{\mathrm{fs}}$ at the interface. If the fluid phase lies to the left of the interface, $(\gamma_+ - \gamma_-) = +1$, otherwise $(\gamma_+ - \gamma_-) = -1$. In single-phase domains, the difference is always zero and the additional source term cancels. The introduction of the phase-identifying functions is especially convenient in handling unit cells with complex interface geometries.

The x-direction interfacial gradient at the fluid side can be obtained from the following equation

$$\left.\frac{\partial \varphi}{\partial x}\right|_{\mathrm{f}} = \frac{\varphi_E - \varphi_P + \gamma_+ - \gamma_-}{x_{e-}/\sigma_{e-} + x_{e+}/\sigma_{e+}} \tag{6f}$$

This equation is used to determine c_{ff} and c_{sf} in Eqs. (5c) and (5d) and the VHTCs in Eqs. (2a)–(2c) in the process of the numerical iteration.

The discretized equations are solved by the line-by-line TDMA algorithm. If, still taking the one-dimensional case for example, the normalized residual

$$R = \frac{\sum_{\text{nodes}} \left(A_W\varphi_W + A_E\varphi_E + Su_P - A_P\varphi_P\right)}{\sum_{\text{nodes}} A_P\varphi_P} < 10^{-6}, \tag{7a}$$

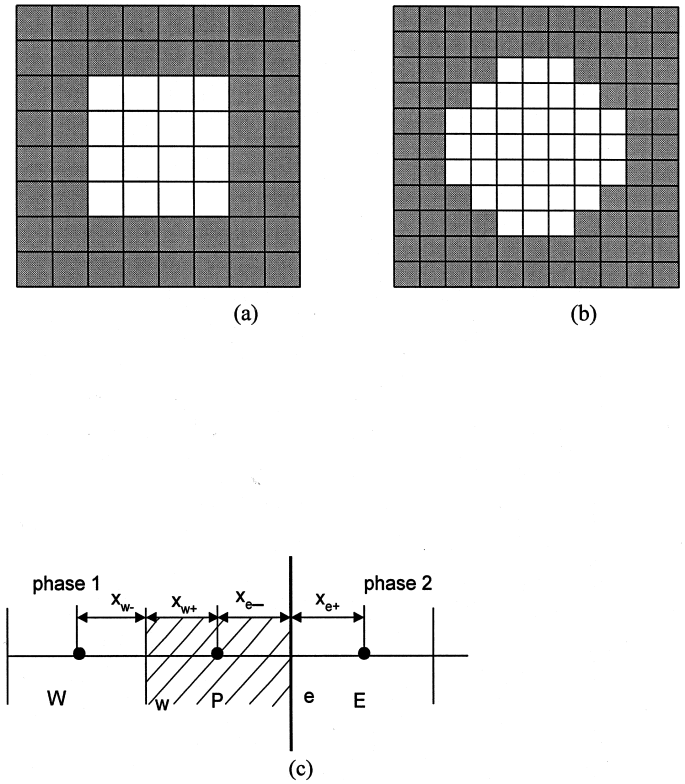

Fig. 2. Schematic of (a) the grid system for case RR; (b) the grid system for case RC and (c) the control volume P with the interface being in position e.

and the relative change in H between the successive iterations satisfies

$$\left|\frac{H^{i+1}-H^{i}}{H^{i+1}}\right| < 10^{-6}, \tag{7b}$$

the numerical iteration is viewed to converge to the solution. If the convective term is considered, the power law profile is introduced to ensure positive coefficients in the discretized equation. The detail of this technique was shown in [8]. For the periodic conditions, the computation is performed over an extended domain. Further detail can be found in [9].

2.3. Numerical results

Here we present the VHTC results for the case without a tortuous flow, some of which will be used in the later sections. Due to symmetry, the computation is conducted over one quarter of a two-dimensional unit cell or one eighth of a three-dimensional unit cell. A numerical test for two- and three-dimensional unit cells has been performed and the results for H_f and H are listed in Table 1. The ε_f for each case is 0.25 except for the three-dimensional hexagonal array case where $\varepsilon_f = 0.395$. We set $\kappa = 10^8$ in the infinite conductivity ratio case. Available analytical solutions are also shown in Table 1 for comparison. It is noted that the present numerical results with the finest grid size listed in the table for each case are accurate enough, even for unit cells with circular and spherical fluid domains. In the followings, the results from the calculation with the finest grid size for each case are presented.

The results of the VHTC H for two-dimensional unit cells at different ε_f and κ are plotted in Fig. 3. For the purpose of comparison, square unit cells with the same volume, $V = \pi r_1^2 = l^2$, are used. The VHTCs from the analytical solution for case CC, (Eq. (3)), are also shown in Fig. 3. It is seen that the VHTC increases with the thermal conductivity ratio for all the unit cells. It is worthy pointing out that a larger VHTC for case RR is due to the larger heat exchange area, which is $(2/\sqrt{\pi}-1) = 12.8\%$ higher than the other two cases at the same volume. Specifically, the VHTC results for case RC with $\varepsilon_f = 0.77$, where the critical volume fraction for the RC is nearly attained, are significantly smaller than those for case CC at low and moderate conductivity ratios.

Fig. 4 shows the effective thermal conductivity for these unit cells. The results can be used to obtain the conductivity components in the energy equations proposed in Section 4. It is found that the effective thermal conductivities for the three unit cells increase with the conductivity ratios and, at large conductivity ratios, this increase becomes linear. Generally a close agreement is found for the three kinds of unit cells. While for case RC with $\varepsilon_f = 0.77$, the discrepancy is observed when κ is far different from 1.

The results of the VHTC H for a three-dimensional unit cell, the hexagonal spherical array, are shown in Fig. 5, in which the results obtained from the idealized three-dimensional sphere array [4] are also shown for comparison, together with the available experimental value for a nylon–water system [5]. Compared with the reported numerical result $H = 11.2$ [5], the present result ($H = 10.5$) is closer to the experimental value.

Table 1
Numerical results of the VHTC for different grid sizes and unit cells

Cases	Conductivity ratio	Grid size	Calculated H_f	Analytical result
RR	1	42×42	2.7832	2.7872 (Eq. (17))
		82×82	2.7870	
	∞	42×42	7.0964	7.1136 (Eq. (18b))
		82×82	7.1092	
RC	1	42×42	3.417	–
		62×62	3.402	
		92×92	3.408	
	∞	42×42	8.113	8 (Eq. (3))
		62×62	8.036	
		92×92	8.036	
Three-dimensional unit cell with cubic fluid domain	∞	$22 \times 22 \times 22$	12.203	12.396 (Eq. (19))
		$32 \times 32 \times 32$	12.309	
		$42 \times 42 \times 42$	12.347	
Three-dimensional unit cell with spherical fluid domain	∞	$32 \times 32 \times 32$	15.16	15 [4]
		$62 \times 62 \times 62$	15.08	
Three-dimensional hexagonal array	0.46	$42 \times 42 \times 42$	$H = 10.49$	Experiment: 8.0 [5]
		$62 \times 62 \times 62$	$H = 10.50$	

3. Thermal analysis

Although the closure problem and the VHTC have been solved by the numerical method in the previous section, their thermal nature is so far not well discussed and understood. The ψ variable is rather a mathematical quantity than the one related to the thermal energy, or the temperature concept. In this section, a thermal analysis will be presented and the thermal nature of the VHTC will be interpreted by the analogous heat transfer cases. This analysis, on the other hand, helps bridge the mathematically formulated VHTC with practical heat exchange situations.

The thermal analysis begins with the temperature decomposition in the VAM. The point temperature for each phase over a representative elementary volume is assumed to be the sum of the intrinsic average temperature and the deviation temperature, i.e.,

$$T_{\mathrm{f}} = \langle T_{\mathrm{f}} \rangle^{\mathrm{f}} + T'_{\mathrm{f}} \tag{8a}$$

$$T_{\mathrm{s}} = \langle T_{\mathrm{s}} \rangle^{\mathrm{s}} + T'_{\mathrm{s}}. \tag{8b}$$

The deviation temperatures can be expanded in terms of macroscopic temperature fields:

$$T'_{\mathrm{f}} = \boldsymbol{b}_{\mathrm{ff}} \cdot \nabla \langle T_{\mathrm{f}} \rangle^{\mathrm{f}} + \boldsymbol{b}_{\mathrm{fs}} \cdot \nabla \langle T_{\mathrm{s}} \rangle^{\mathrm{s}} + \psi_{\mathrm{f}} \left(\langle T_{\mathrm{s}} \rangle^{\mathrm{s}} - \langle T_{\mathrm{f}} \rangle^{\mathrm{f}} \right) \tag{9a}$$

$$T'_{\mathrm{s}} = \boldsymbol{b}_{\mathrm{sf}} \cdot \nabla \langle T_{\mathrm{f}} \rangle^{\mathrm{f}} + \boldsymbol{b}_{\mathrm{ss}} \cdot \nabla \langle T_{\mathrm{s}} \rangle^{\mathrm{s}} + \psi_{\mathrm{s}} \left(\langle T_{\mathrm{s}} \rangle^{\mathrm{s}} - \langle T_{\mathrm{f}} \rangle^{\mathrm{f}} \right) \tag{9b}$$

The truncated terms in the above expansion have been shown to be negligible for relatively large time behavior in the cases of pure heat conduction [2,4]. $\boldsymbol{b}_{\mathrm{ff}}$, $\boldsymbol{b}_{\mathrm{fs}}$, $\boldsymbol{b}_{\mathrm{sf}}$ and $\boldsymbol{b}_{\mathrm{ss}}$ are thermal-conductivity-related closure

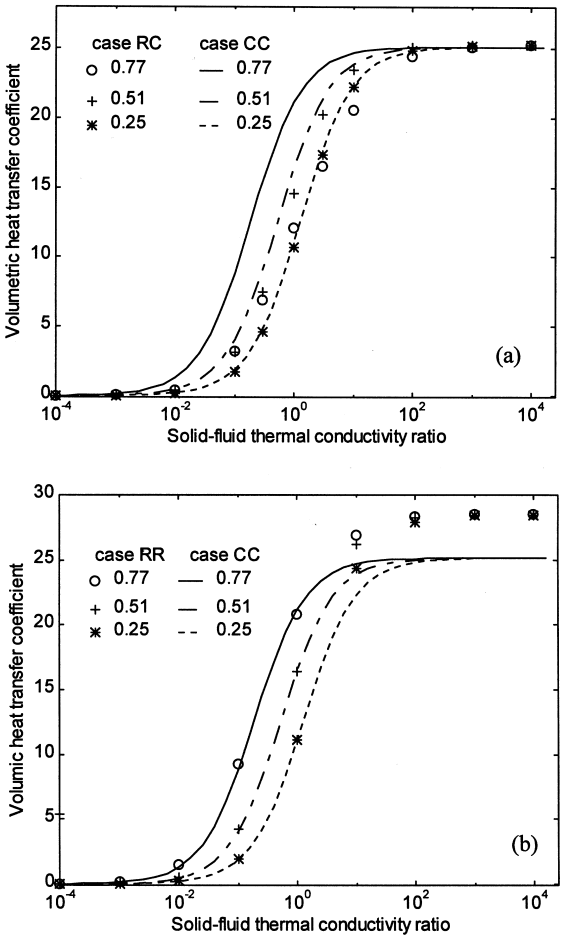

Fig. 3. Volumetric heat transfer coefficients vs. solid–fluid thermal conductivity ratios at different ε_{f} (0.25. 0.51 and 0.77): (a) comparison of cases RC and CC; (b) comparison of cases RR and CC.

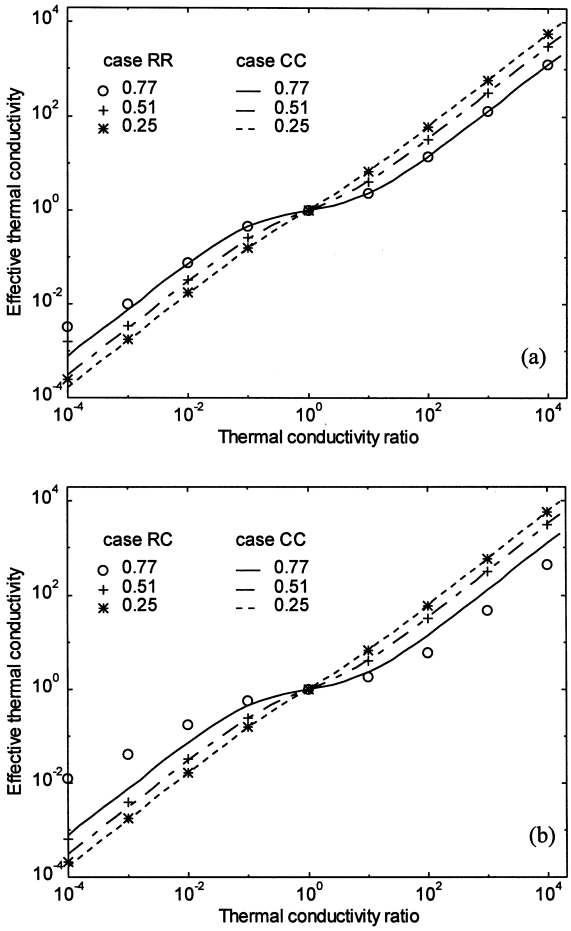

Fig. 4. Effective thermal conductivities vs. solid–fluid thermal conductivity ratios at different ε_{f}: (a) comparison of cases RR and CC; (b) comparison of cases RC and CC.

variables, known as $\boldsymbol{b}$ variables in the VAM. More detail on the $\boldsymbol{b}$ variables can be found in [1,2,10–12]. Here we emphasize on the ψ field and the VHTC.

The deviation temperatures T'_{f} and T'_{s} in Eqs. (9a) and (9b) are, respectively, composed of three parts: the contribution due to the macroscopic solid temperature gradient, denoted by T'_{f1} and T'_{s1}; the contribution due to the macroscopic fluid temperature gradient, T'_{f2} and T'_{s2}; and the contribution due to the phasic temperature difference, T'_{f3} and T'_{s3}. In the absence of macroscopic temperature gradients, the deviation temperatures are related only to the phasic temperature difference and the point temperatures, Eqs. (8a) and (8b), reduce to

$$T_{\mathrm{f}} = \langle T_{\mathrm{f}}\rangle^{\mathrm{f}} + T'_{\mathrm{f3}}, \tag{10a}$$

$$T_{\mathrm{s}} = \langle T_{\mathrm{s}}\rangle^{\mathrm{s}} + T'_{\mathrm{s3}}. \tag{10b}$$

Multiplying Eqs. (1a)–(1f) by the macroscopic temperature difference $(\langle T_{\mathrm{s}}\rangle^{\mathrm{s}} - \langle T_{\mathrm{f}}\rangle^{\mathrm{f}})$ and noticing that $T'_{\mathrm{f3}} = \psi_{\mathrm{f}}(\langle T_{\mathrm{s}}\rangle^{\mathrm{s}} - \langle T_{\mathrm{f}}\rangle^{\mathrm{f}})$ and $T'_{\mathrm{s3}} = \psi_{\mathrm{s}}(\langle T_{\mathrm{s}}\rangle^{\mathrm{s}} - \langle T_{\mathrm{f}}\rangle^{\mathrm{f}})$, one obtains the equations for the deviation temperatures as

$$\left[(\rho c)_{\mathrm{f}}\langle \boldsymbol{u}\rangle^{\mathrm{f}}\cdot\nabla T'_{\mathrm{f3}}\right] = \nabla\cdot\left(k_{\mathrm{f}}\nabla T'_{\mathrm{f3}}\right) - \frac{k_{\mathrm{f}}}{V_{\mathrm{f}}}\int \boldsymbol{n}_{\mathrm{fs}}\cdot\nabla T'_{\mathrm{f3}}\,\mathrm{d}A_{\mathrm{fs}} \tag{11a}$$

$$0 = \nabla\cdot\left(k_{\mathrm{s}}\nabla T'_{\mathrm{s3}}\right) - \frac{k_{\mathrm{s}}}{V_{\mathrm{s}}}\int \boldsymbol{n}_{\mathrm{sf}}\cdot\nabla T'_{\mathrm{s3}}\,\mathrm{d}A_{\mathrm{fs}} \tag{11b}$$

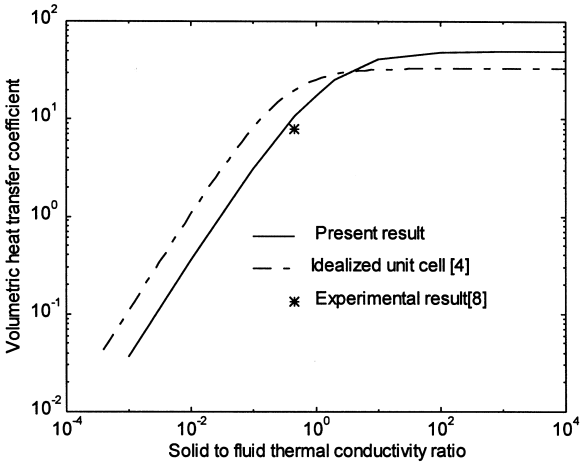

Fig. 5. Volumetric heat transfer coefficients vs. solid–fluid thermal conductivity ratios for three-dimensional unit cells.

$$\begin{aligned} &T'_{\mathrm{f3}} = T'_{\mathrm{s3}} + \langle T_{\mathrm{s}}\rangle^{\mathrm{s}} - \langle T_{\mathrm{f}}\rangle^{\mathrm{f}},\\ &\boldsymbol{n}_{\mathrm{fs}}\cdot k_{\mathrm{f}}\nabla T'_{\mathrm{f3}} = \boldsymbol{n}_{\mathrm{fs}}\cdot k_{\mathrm{s}}\nabla T'_{\mathrm{s3}} \quad \text{at } A_{\mathrm{fs}} \end{aligned} \tag{11c}$$

$$T'_{\mathrm{f3}}(\boldsymbol{r}+\boldsymbol{l}) = T'_{\mathrm{f3}}(\boldsymbol{r}), \qquad T'_{\mathrm{s3}}(\boldsymbol{r}+\boldsymbol{l}) = T'_{\mathrm{s3}}(\boldsymbol{r}). \tag{11d}$$

Here the phasic temperature difference $(\langle T_{\mathrm{s}}\rangle^{\mathrm{s}} - \langle T_{\mathrm{f}}\rangle^{\mathrm{f}})$ has been assumed to be a constant over the representative volume. In the absence of the spatial temperature gradients, by using Eqs. (10a) and (10b), Eqs. (11a)–(11d) can be written as

$$\langle \boldsymbol{u}\rangle^{\mathrm{f}}\cdot\nabla T_{\mathrm{f}} = \nabla\cdot(\alpha_{\mathrm{f}}\nabla T_{\mathrm{f}}) - \frac{\alpha_{\mathrm{f}}}{V_{\mathrm{f}}}\int \boldsymbol{n}_{\mathrm{fs}}\cdot\nabla T_{\mathrm{f}}\,\mathrm{d}A_{\mathrm{fs}} \tag{12a}$$

$$0 = \nabla\cdot(\alpha_{\mathrm{s}}\nabla T_{\mathrm{s}}) - \frac{\alpha_{\mathrm{s}}}{V_{\mathrm{s}}}\int \boldsymbol{n}_{\mathrm{sf}}\cdot\nabla T_{\mathrm{s}}\,\mathrm{d}A_{\mathrm{fs}} \tag{12b}$$

$$T_{\mathrm{f}} = T_{\mathrm{s}}, \qquad \boldsymbol{n}_{\mathrm{fs}}\cdot k_{\mathrm{f}}\nabla T_{\mathrm{f}} = \boldsymbol{n}_{\mathrm{fs}}\cdot k_{\mathrm{s}}\nabla T_{\mathrm{s}} \quad \text{at } A_{\mathrm{fs}} \tag{12c}$$

$$T_{\mathrm{f}}(\boldsymbol{r}+\boldsymbol{l}) = T_{\mathrm{f}}(\boldsymbol{r}), \qquad T_{\mathrm{s}}(\boldsymbol{r}+\boldsymbol{l}) = T_{\mathrm{s}}(\boldsymbol{r}). \tag{12d}$$

In the above equations, the temperature gradients ∇T_{f} and ∇T_{s} are referred to as the microscopic temperature gradients which are meaningful within the unit cell. They are different from the temperature gradients $\nabla\langle T_{\mathrm{f}}\rangle^{\mathrm{f}}$ and $\nabla\langle T_{\mathrm{s}}\rangle^{\mathrm{s}}$ at the macroscopic level. It is seen that the closure problem has been reversibly transformed into an analogous thermal problem in terms of point temperatures. With the similar procedure, Eqs. (2a)–(2c) can also be expressed

$$H = \frac{1}{\langle T_{\mathrm{s}}\rangle^{\mathrm{s}} - \langle T_{\mathrm{f}}\rangle^{\mathrm{f}}}\frac{l^2}{V}\int \boldsymbol{n}_{\mathrm{fs}}\cdot\nabla T_{\mathrm{f}}\,\mathrm{d}A_{\mathrm{fs}}, \tag{13a}$$

$$H_{\mathrm{f}} = \frac{1}{\langle T_{\mathrm{s}}\rangle^{\mathrm{s}} - \langle T_{\mathrm{f}}\rangle^{\mathrm{f}}}\frac{l_{\mathrm{f}}^2}{V_{\mathrm{f}}}\int \boldsymbol{n}_{\mathrm{fs}}\cdot\nabla T_{\mathrm{f}}\,\mathrm{d}A_{\mathrm{fs}}, \tag{13b}$$

$$H_{\mathrm{f}} = \frac{1}{\langle T_{\mathrm{s}}\rangle^{\mathrm{s}} - \langle T_{\mathrm{f}}\rangle^{\mathrm{f}}}\frac{r_0^2}{V_{\mathrm{f}}}\int \boldsymbol{n}_{\mathrm{fs}}\cdot\nabla T_{\mathrm{f}}\,\mathrm{d}A_{\mathrm{fs}}. \tag{13c}$$

Namely the VHTC is also reformulated in terms of point temperatures. Since $\boldsymbol{n}_{\mathrm{fs}}\cdot\nabla T_{\mathrm{f}}$ multiplied by k_{f} defines the heat flux, the VHTC is thus physically interpreted as the dimensionless average heat flux at the interface. Based on the analogous thermal problem, Eqs. (12a)–(12d), the VHTC can be found directly by the means of thermal analysis, instead of resorting to the mathematically formulated closure equations (1a)–(1f). We present two cases to further illustrate the thermal analysis and, simultaneously, examine the thermal nature of the VHTC.

3.1. Case 1: circular two-phase domain

The circular domain is shown in Fig. 1(c), which corresponds to case CC. The solution of the VHTC has been shown in Eq. (3). As the conductivity ratio κ approaches infinity, the maximum value $H_f = 8$ ($H = 8\pi$) is attained. This can be understood as the Nusselt number for the classical heat transfer case in which a uniform heat flux is imposed from the wall to the fluid flowing in a circular tube with a uniform velocity profile. At a finite conductivity ratio, the analogous thermal problem derived from Eqs. (12a)–(12d) is

$$\frac{1}{r}\frac{\partial}{\partial r}\left(r\frac{\partial T_f}{\partial r}\right) = 2 \quad 0 \le r \le 1 \tag{14a}$$

$$\frac{1}{r}\frac{\partial}{\partial r}\left(r\frac{\partial T_s}{\partial r}\right) = -\frac{2}{\kappa\left[(r_1/r_0)^2-1\right]} \quad 1 \le r \le r_1/r_0 \tag{14b}$$

where the temperatures T_f and T_s have been non-dimensionalized by the characteristic temperature qr_0/k_f with q being the heat flux through the solid–fluid interface at $r = 1$. The solution of the temperature field is

$$T_f(r) = T_{fs} - \frac{1}{2}(1 - r^2) \quad 0 \le r \le 1 \tag{14c}$$

$$T_s(r) = T_{fs} + \frac{(r_1/r_0)^2}{\kappa\left[(r_1/r_0)^2-1\right]}\ln r - \frac{1}{2\kappa\left[(r_1/r_0)^2-1\right]}(r^2 - 1) \tag{14d}$$

$1 \le r \le r_1/r_0$.

Here T_{fs} denotes the temperature at the solid–fluid interface and is set to be zero since it is only a reference temperature. According to Eq. (13c), the VHTC can be written as

$$H_f = \frac{2}{\langle T_s\rangle^s - \langle T_f\rangle^f} = \frac{8}{1 + \left(-2\ln\varepsilon_f - 2\varepsilon_s - \varepsilon_s^2\right)/\varepsilon_s^2\kappa}. \tag{15a}$$

This result is identical to Eq. (3). Namely the same VHTC is obtained from the analogous heat transfer case. The profile for the temperatures reduced by the temperature difference ($\langle T_s\rangle^s - \langle T_f\rangle^f$) has been shown in Fig. 6(a) for different conductivity ratios. Reversing the thermal analysis procedure, we can obtain the ψ field from the temperature solution. The corresponding profile is shown in Fig. 6(b). It is observed that the difference of the two profiles lies in the value jump at the interface. The gradient-dependent VHTCs from the closure problem and the analogous thermal energy equations are the same.

It is interesting to derive H_f for the analogous thermal problem with a non-uniform velocity field — fully developed flow in the circular tube. In this case, the non-dimensional heat consumption term on the right-hand side of Eq. (14a) becomes $4(1 - r^2)$ instead of 2 in the fluid domain. The VHTC takes the form

$$H_f = \frac{8}{4/3 + \left(-2\ln\varepsilon_f - 2\varepsilon_s - \varepsilon_s^2\right)/\varepsilon_s^2\kappa} \tag{15b}$$

where the factor 4/3 instead of 1 appears in the denominator and the heat transfer rate is, therefore, decreased. This suggests that a smaller heat transfer coefficient is expected if non-uniform velocity field is taken into account.

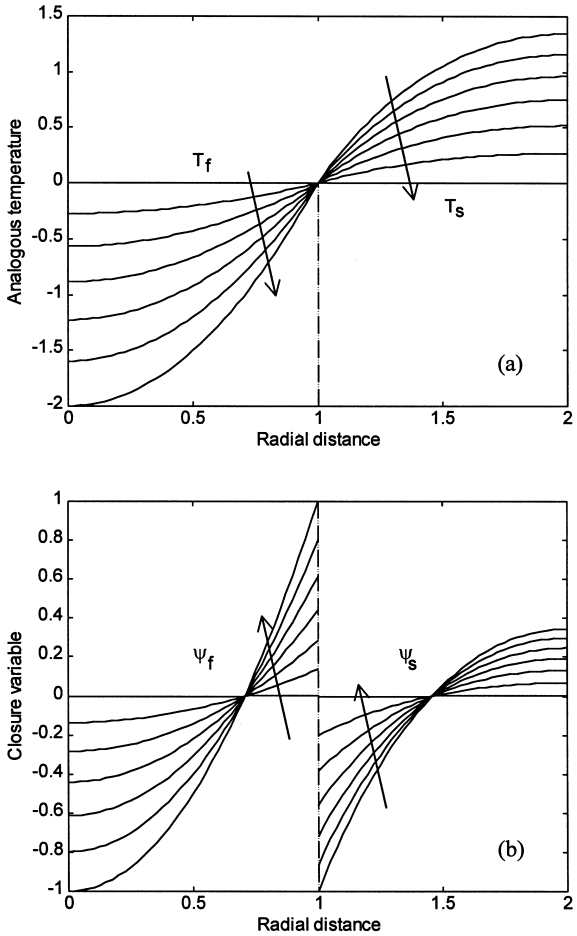

Fig. 6. Results of (a) the temperature profile and (b) the closure variable for case CC, with solid to fluid conductivity ratios arranged in the order shown by the arrows as: 0, 0.2, 0.5, 1, 2, 5, $+\infty$.

3.2. Case 2: rectangular two-phase domain

We consider the analogous thermal problem over a rectangular two-phase domain. The coordinate system is shown in Fig. 7. For such geometry, we consider two special cases: $\kappa = 1$ and $\kappa \to \infty$, for which the analytical solutions of the analogous thermal energy equations can be found.

When $\kappa = 1$, there is no jump in the temperature gradient. We assume the spatial average temperature $\langle T \rangle = 0$. The dimensionless thermal balance equation with uniform heat generation in the solid and heat consumption in the fluid is

$$\frac{\partial^2 T}{\partial y^2} + \frac{\partial^2 T}{\partial z^2} = \begin{cases} 1 & 0 \le y \le a \text{ and } 0 \le z \le b \\ -\dfrac{ab}{\beta} & 0 \le y \le a \text{ and } b \le z \le \beta, \\ & \text{or } a \le y \le 1 \text{ and } b \le z \le \beta \end{cases}$$

The boundaries are all thermally insulated. By using Green's functions one can obtain the temperature profile as

$$T = -\frac{2b\beta}{\beta - ab}\sum_{m=1}^{\infty}\frac{\cos(\beta_m y)\sin(\beta_n a)}{\beta_m^3} - \frac{2a\beta^3}{\beta - ab}\sum_{n=1}^{\infty}\frac{\cos(\beta_n z/b)\sin(\beta_n b/\beta)}{\beta_n^3} - 4\frac{\beta}{\beta - ab}\sum_{m=1}^{\infty}\sum_{n=1}^{\infty} \times \frac{(-1)^{m+n}\cos(\beta_m y)\cos(\beta_n z/\beta)\sin(\beta_m a)\sin(\beta_n b/\beta)}{\beta_m\beta_n\left[\beta_m^2 + (\beta_n/\beta)^2\right]} \tag{16}$$

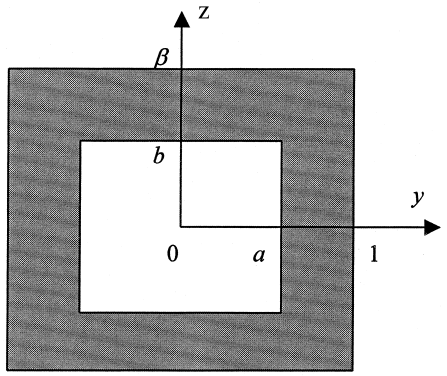

Fig. 7. Coordinate system for the thermal analysis of case RR.

with $\beta_m = m\pi$, $\beta_n = n\pi$ and m, n are positive integers. The temperature has been non-dimensionalized by the characteristic temperature $(a+b)ql_s(k_f ab)^{-1}$ with q being the averaged heat flux through the interface. With Eq. (13b) the heat transfer coefficient H_f can be expressed as

$$H_f = (ab/\beta)\left\{\frac{2b\beta^2}{a(\beta - ab)^2}\sum_{m=1}^{\infty}\frac{\sin^4(\beta_m a)}{\beta_m^4} + \frac{2a\beta^5}{b(\beta - ab)^2}\sum_{n=1}^{\infty}\frac{\sin^2(\beta_n b/\beta)}{\beta_n^4} + \frac{4\beta^3}{ab(\beta - ab)^2}\sum_{m=1}^{\infty}\sum_{n=1}^{\infty}\frac{\sin^2(\beta_m a)\sin^2(\beta_n b/\beta)}{\beta_m^2\beta_n^2\left[\beta_m^2 + (\beta_n/\beta)^2\right]}\right\}^{-1} \tag{17}$$

For $\beta = 1$ and $a = b = 1/2$, Eq. (17) yields $H_f = 2.7872$. This value is very close to the numerical result 2.7870 with a 82×82 grid system as listed in Table 1. The temperature profile based on the analytical solution is shown in Fig. 8(a). The closure variables can be reversibly obtained from the thermal analysis. The corresponding ψ profile is displayed in Fig. 8(b).

As $\kappa \to \infty$, the solid temperature is uniform and only the temperature field in the fluid domain is meaningful. For simplicity we take $a = 1$ and $b = \beta$. Again we set the reference temperature $T_{fs} = 0$. The solution for the analogous thermal problem with uniform heat consumption in the fluid is

$$T_f = -\frac{4(1+\beta)}{\beta}\sum_{m=1}^{\infty}\sum_{n=1}^{\infty}\frac{(-1)^{m+n}\cos(\beta_m y)\cos(\beta_n z)}{\beta_m^2\beta_n^2\left[\beta_m^2 + (\beta_n/\beta)^2\right]} \tag{18a}$$

where $\beta_m = (m - 1/2)\pi$ and $\beta_n = (n - 1/2)\pi$. The temperature has been non-dimensionalized by the characterized temperature ql_f/k_f. The heat transfer coefficient is obtained as

$$H_f = \left\{4\sum_{m=1}^{\infty}\sum_{n=1}^{\infty}\frac{1}{\beta_m^2\beta_n^2\left[\beta_m^2 + (\beta_n/\beta)^2\right]}\right\}^{-1}. \tag{18b}$$

For a square unit cell, i.e., $\beta = 1$, the result of H_f is 7.1136. This value agrees with the calculated result 7.1092 in Table 1. If β approaches infinity, i.e., a stratified system, $H_f \to 3$.

In the three-dimensional case with cubic fluid domain, the H_f at $\kappa \to \infty$ is given by

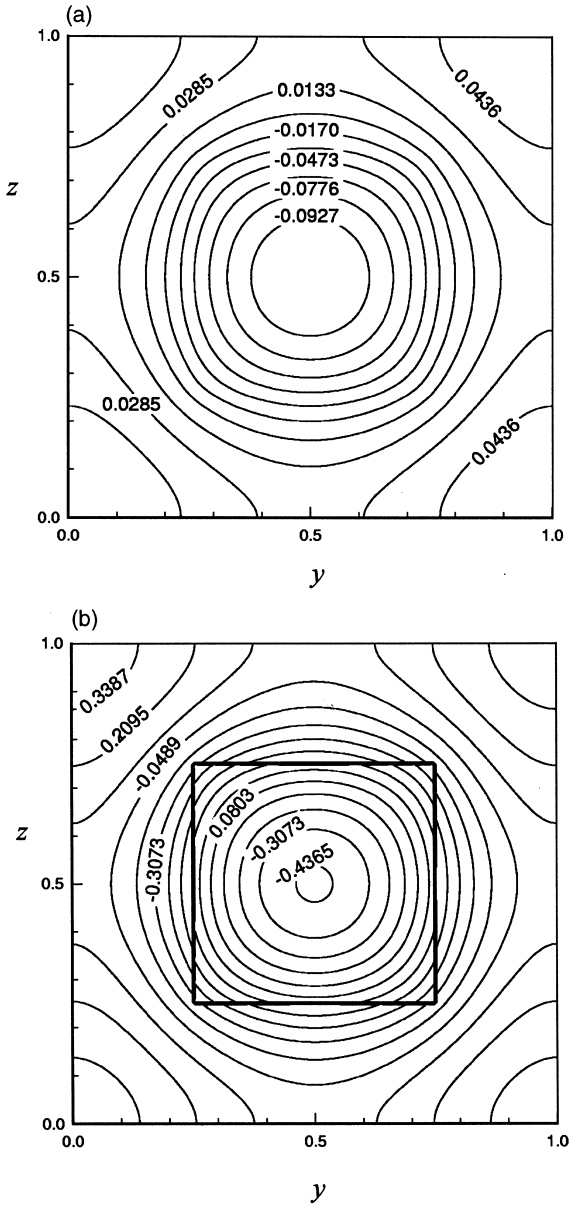

Fig. 8. Results for case RR with $\kappa = 1$: (a) temperature profile; (b) closure variable.

$$H_{\mathrm{f}} = \left\{ 8 \sum_{m=1}^{\infty} \sum_{n=1}^{\infty} \sum_{p=1}^{\infty} \frac{1}{\beta_m^2 \beta_n^2 \beta_p^2 \left(\beta_m^2 + \beta_n^2 + \beta_p^2 \right)} \right\}^{-1} \tag{19}$$

where $\beta_m = (m - 1/2)\pi$, $\beta_n = (n - 1/2)\pi$ and $\beta_p = (p - 1/2)\pi$. The converged value is 12.396. The numerical result with a $42 \times 42 \times 42$ grid system is 12.347. Consistency is achieved for the closure formulation and the thermal analogy formulation.

The thermal analysis of the VHTC is especially useful in initiating the modification of the VHTC. In conventional VAM modeling, the VHTC as well as other transport coefficients is assumed to be constant throughout the porous medium and can be obtained by the closure formulation or the thermal analogy formulation. Its applicability, however, is within the modeling limitation such as the small Peclet number constraint (this will be discussed in the next section). In a finite-size porous system with large Peclet number, this constraint will be violated and efforts should be made on the modification of such a transport coefficient. Inferred from the thermal analysis, the modification could be made by taking into account the analogous heat transfer at the unit-cell level. At this microscopic level, the heat transfer occurs in a manner being different from the conventional VAM modeling with a constant VHTC. In contrast, the VHTC is a variable quantity along the flow direction due to the thermal entrance effect. On the other hand, the non-uniformity of the flow field will cause a smaller asymptotic VHTC as seen in the foregoing discussion. In the next section, an improved VHTC model is discussed in detail.

4. Improved VHTC model with fluid flow

4.1. Limitations of the VAM with fluid flow

In the case of convection heat transfer, the validity of the VAM with the closure formulation is restricted to low and moderate microscopic Peclet number Pe_l, as reported by the present authors [7]. Such limitations are inherent from the VAM. In the self-contained development of this methodology, porous media are assumed homogeneous and the local temperature expansions (Eqs. (9a) and (9b)) are valid everywhere in the system. If the fluid flow is considered, the following Peclet number criterion should be satisfied [7]:

$$Pe_l = \frac{\langle u \rangle^{\mathrm{f}} l}{\alpha_{\mathrm{f}}} \ll \frac{L}{l}.$$

i.e., the microscopic Peclet number should be much smaller than the macroscopic to microscopic length ratio so that the VAM could be valid. At large Peclet number Pe_l, this criterion is easily violated and the local average scheme given in Eqs. (9a) and (9b) may break down, especially at or around the thermal entrance region of a porous heat transfer system. Furthermore, the additional convective terms in the VAM, due to non-uniformity of the velocity field, will produce a result that does not coincide with the energy conservation [1,6].

4.2. Improved VHTC model

We attempt to improve the VHTC model so that it may be extended to larger Peclet number. It was reported [7] that the solid temperature at the entrance region, where x is smaller, is larger than the predicted result from the point equations while the fluid temperature is underestimated. Maintaining the thermal conductivity components unchanged, this observation indicates that the VHTC is larger at the smaller x. If turning to the microscopic heat transfer that occurs in a straight channel, as suggested by the thermal analysis, and knowing that a large heat transfer coefficient at a small x corresponds to the thermal entrance phenomenon, we may reconsider the VHTC as a function of x following the thermal entrance theory [13]. Namely

$$H(x) = c_0 H f(x) \tag{20}$$

where c_0 is a constant, which is less than one as a result of the non-uniformity of the velocity field, H is the original VHTC in the VAM and can be read out from Fig. 3, and $f(x)$ is a modification function based on the thermal entrance phenomenon and is given as

$$f(x) = \frac{Nu_x}{Nu_x|_{x\to\infty}} \tag{21}$$

Since the Nusselt number correlations for rectangular ducts are not available [13], we make use of the thermal entrance heat transfer result generated from a circular tube. The determination of the local Nusselt number Nu_x and the Nusselt number $Nu_x|_{x\to\infty}$ for a circular tube can be found in [13]. For the two dimensional porous system shown in Fig. 9(a), the energy equations in dimensionless form are proposed as follows:

In the solid phase

$$\varepsilon_f Pe_L \frac{\partial T_f}{\partial x} = \varepsilon_f \frac{\partial^2 T_f}{\partial x^2} + \frac{K_{ff,\,zz}}{k_f}\frac{\partial^2 T_f}{\partial z^2} + \frac{K_{fs,\,zz}}{k_f}\frac{\partial^2 T_s}{\partial z^2} + \left(\frac{L}{l}\right)^2 H(x)(T_s - T_f) \tag{22a}$$

In the fluid phase

$$0 = \varepsilon_s \kappa \frac{\partial^2 T_s}{\partial x^2} + \frac{K_{ss,\,zz}}{k_f}\frac{\partial^2 T_s}{\partial z^2} + \frac{K_{sf,\,zz}}{k_f}\frac{\partial^2 T_f}{\partial z^2} + \left(\frac{L}{l}\right)^2 H(x)(T_f - T_s) \tag{22b}$$

Here intrinsic average operators $\langle\rangle^f$ and $\langle\rangle^s$ have been omitted for brevity. The dimensionless temperatures take the following form

$$T_f = \frac{T_f^* - T_{in}^*}{T_{wall}^* - T_{in}^*}, \qquad T_s = \frac{T_s^* - T_{in}^*}{T_{wall}^* - T_{in}^*}$$

The superscript '*' has been used to denote the dimensional temperatures, and T_{wall}^* and T_{in}^* are the temperatures of the hot surface and the inlet fluid. The macroscopic Peclet number Pe_L is defined by the macroscopic length L_z. The terms containing the conductivity components $K_{ff,\,zz}$, $K_{fs,\,zz}$, $K_{ss,\,zz}$ and $K_{sf,\,zz}$ represent the conductive effects in z direction due to the lateral heating. They can be obtained numerically or experimentally according to the VAM theory, for instance, in [2]. Further detail can be found in [10–12]. The calculation of these conductivity components for the present modeling has been shown in the Appendix. ($K_{ss,\,zz}$ seems much larger than the other conductivity components. However, we retain all these terms to be consistent with the VAM). The additional convective terms in the VAM are removed from Eqs. (22a) and (22b) to meet the energy conservation requirement.

For case RR shown in Fig. 9(b), the constant c_0 in Eq. (20) is about 0.50 for isothermal boundary conditions, which is found by fitting the overall averaged solid temperature or the mixed mean fluid temperature from the modified model with that from the point-wise modeling. This value is a little different from the result for a circular tube case (0.75 for $\kappa = 1000$). The modified VHTC model is shown in Fig. 10 in comparison with the original VHTC model.

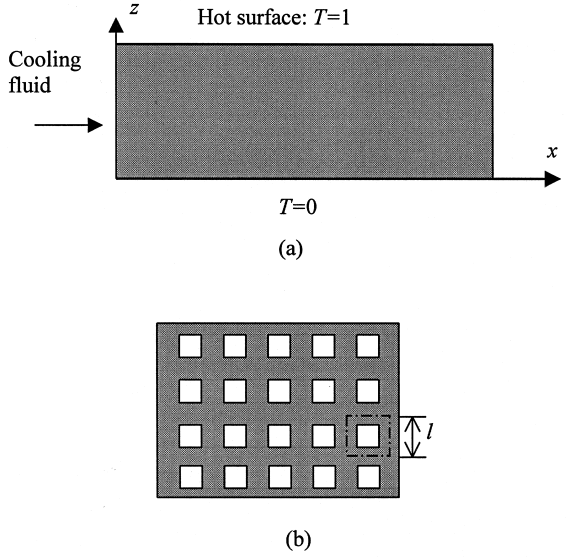

Fig. 9. A porous medium model with fluid flowing through straight rectangular ducts: (a) the heat transfer system; (b) the porous cross sections vertical to the flow direction.

4.3. Numerical modeling and verification

The modified VHTC model is still an empirical one. Its validity is examined by comparing the results from the point equations. The porous system characterized by straight rectangular ducts is selected, as shown in Fig. 9, with the representative unit cell corresponding to the RR case defined in the foregoing section. The selection of such pore structure renders less effort for the point-wise modeling due to the regularity of the geometry while the computational accuracy is ensured. Ten unit cells are employed in z direction so that $l/L \ll 1$. The fluid flow is assumed uniformly fully-developed at the inlet of each duct. Once the three-dimensional point temperature fields are obtained, the averaged temperatures can be calculated by the following equations:

$$T_{\mathrm{f}}(x) = \frac{1}{\langle u\rangle^{\mathrm{f}} L_y L_z} \int T_{\mathrm{f}}(x, y, z) u(y, z)(1-\gamma)\,\mathrm{d}y\,\mathrm{d}z, \quad (23a)$$

$$T_{\mathrm{s}}(x, z) = \frac{1}{L_y} \int T_{\mathrm{s}}(x, y, z)\gamma\,\mathrm{d}y, \quad (23b)$$

$$T_{\mathrm{s}}(x) = \frac{1}{L_y L_z} \int T_{\mathrm{s}}(x, y, z)\gamma\,\mathrm{d}y\,\mathrm{d}z, \quad (23c)$$

where γ is the phase-identifying function defined in the same form as Eq. (4a), with the phasic domain of the definition being extended to the overall porous medium system instead of one unit cell.

By comparing with the point-wise modeling, the present model is found to be applicable to convection heat transfer with Pe_l ranging from several tens to several thousands. Thus, the VAM is extended to the overall laminar flow regime if water or air is used as working fluids. In the followings we will show the results with isothermal conditions for the case of $Pe_l = 1000$ with $\kappa = 1000$. This high conductivity ratio is a representative of practical systems with metallic solid matrix, such as copper–water, copper–air, or stainless steel–air systems.

In Fig. 11, the solid and fluid temperature profiles along the flow direction x are presented for the three models: the original VAM modeling, the modified model and the point-wise modeling. It is seen that the deviation of the VAM is significant, while the modified model produces much better results in spite of the local temperature expansion constraints in the VAM.

The details of the solid and fluid temperature fields are shown in Fig. 12. The different temperature profiles for the solid and the fluid suggests the necessity of a two-equation modeling. The span-wise averaged solid temperature profile from the point-wise modeling is also shown in Fig. 12(a) for comparison. As we can see, the agreement is generally fine. It is noted that the dashed lines corresponding to the point-wise modeling are not well smoothed out. This originates from the introduction of a zeroth order weighting function, the phase-identifying function γ into the span-wise averaging of the point temperature field. A higher order weighting function will help smooth out the lines. In the present work, however, the zeroth order weighting averaging seems enough to illustrate the overall agreement of the two models as shown in the figure.

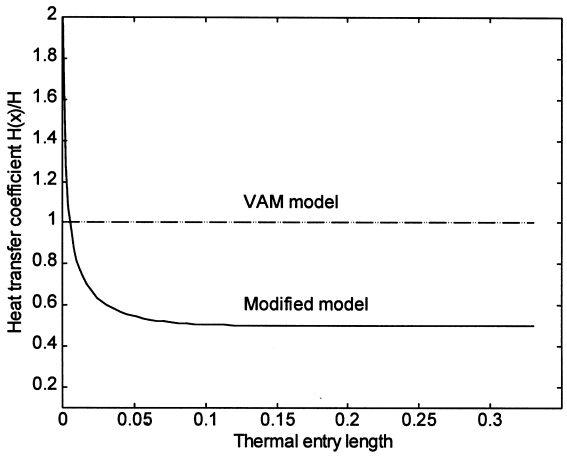

Fig. 10. Comparision of heat transfer coefficient models.

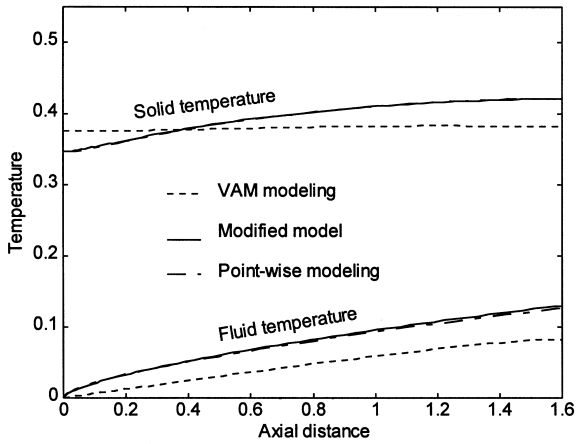

Fig. 11. Solid and fluid temperature profiles vs. the axial distance x/L for different models. The solid temperature profiles for the modified model and the point-wise modeling are very close.

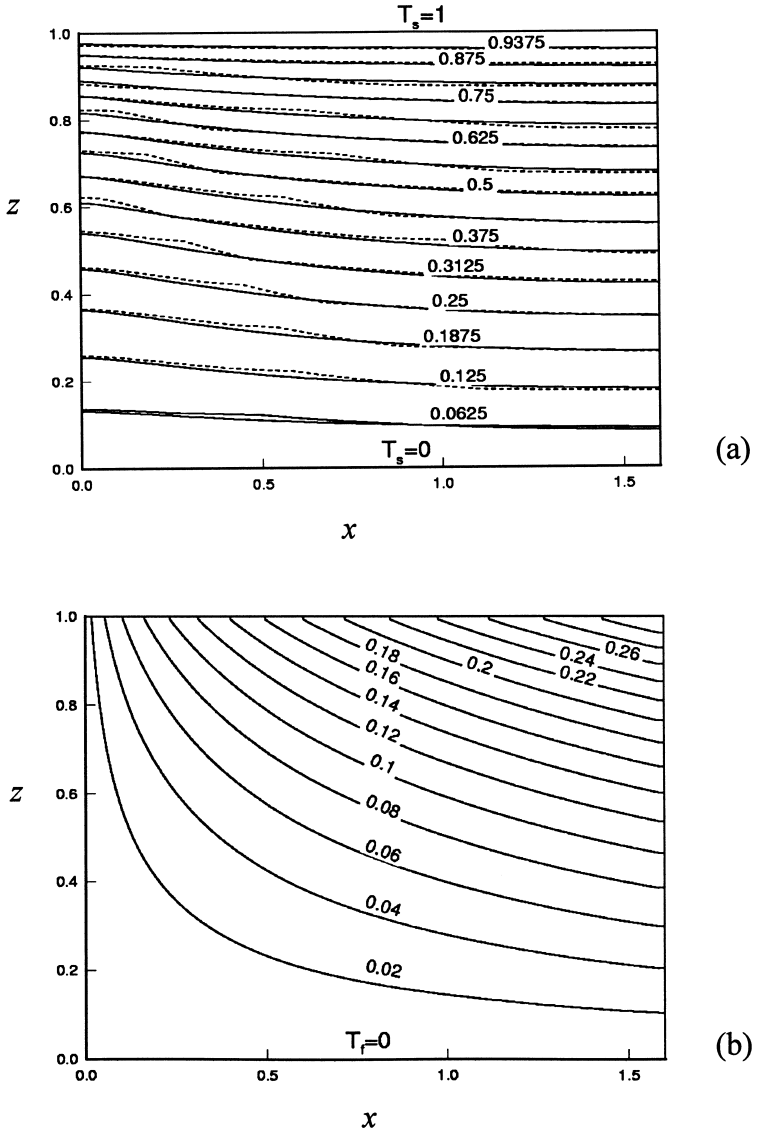

Fig. 12. Temperature profiles based on the modified model: (a) the solid matrix temperature profile and comparision with the point-wise modeling; (b) the fluid temperature profile.

5. Conclusions

The modeling of the VHTC in solid–fluid porous media with consolidated matrix structures has been conducted at the unit-cell level. The value of the VHTC is numerically determined by solving the closure problem developed in the VAM. The control-volume finite difference method is used and the phase-identifying functions are introduced to facilitate the solution over the two-phase domain. The thermal nature of the VHTC is explored by means of thermal analysis. The conclusions can be drawn as follows:

1. The interfacial jump condition in the closure problem can be treated as an additional source term in the discretized equation to simplify the solution procedure. The calculated VHTC results in the present study have been verified with available analytical results and the good agreement has been achieved. The results for the two-dimensional unit cells are found not sensitive to the geometry, while for three-dimensional cases, the VHTCs vary significantly versus the geometry.
2. A thermal analysis of the VHTC is conducted by inspecting the theoretical origin. In this analysis, the

VHTC is interpreted as the dimensionless average heat flux at the interface and the analogous thermal problems with circular and rectangular domains have been examined. The thermal analysis presented in this paper may help to develop more rigorous VHTC models for practical porous medium systems.

3. In the application of the VAM to a forced convection heat transfer in a solid matrix characterized by straight ducts, an improved VHTC model is proposed by incorporating the analogous unit-cell-level heat transfer mechanism, in which the effects of the non-uniformity of the velocity field and the thermal entrance at the microscopic level are taken into account. By comparing with the point-wise modeling, the new VHTC model is found to be able to predict heat transfer for the large Peclet number laminar flow regime with water and air as working fluids. This modeling permits optimization of designing practical porous heat sinks in heat transfer enhancements with greatly reduced modeling efforts. It also suggests an analytical technique for convection heat transfer in porous media with much more complicated structure.

Appendix

Determination of the thermal conductivity components

In the modified VAM modeling, Eqs. (22a) and (22b), the components of the conductivity tensors are related to the thermal tortuosity due to the different phasic conductivities and geometries. They can be evaluated directly from the $\boldsymbol{b}$ variables in the VAM. A theoretical description of the thermal conductivity components has been elaborated in [2]. Here we are not intending to repeat the detailed process since this is not straightforward. We just present how to obtain the conductivity components related to the modeling Eqs. (22a) and (22b) by making use of the effective thermal conductivity tensor $\mathbf{K}_{\text{eff}}$ in the one-equation model.

The relationship between the effective thermal conductivity tensor $\mathbf{K}_{\text{eff}}$ and the tortuosity tensor $\mathbf{B}$ is

$$\mathbf{K}_{\text{eff}}/k_{\text{f}} = \left[\varepsilon_{\text{f}} + (1-\varepsilon_{\text{f}})\kappa\right]\mathbf{I} + \varepsilon_{\text{f}}(1-\kappa)^2\mathbf{B}. \tag{A1}$$

Here the effective conductivity tensor $\mathbf{K}_{\text{eff}}$ corresponds to the one-equation model and can be obtained by the conventional experimental measurement or theoretical calculation over a single unit cell [10]. Considering the zz component, one finds the tortuosity effect from Eq. (A1) as

$$\mathrm{B}_{zz} = \left[\mathrm{K}_{\text{eff},\,zz}/k_{\text{f}} - \varepsilon_{\text{f}} - (1-\varepsilon_{\text{f}})\kappa\right]/\varepsilon_{\text{f}}(1-\kappa)^2 \tag{A2}$$

The conductivity components can be given as

$$\mathrm{K}_{\text{ff},\,zz}/k_{\text{f}} = \varepsilon_{\text{f}}(1+\mathrm{B}_{zz}) \tag{A3}$$

$$\mathrm{K}_{\text{fs},\,zz}/k_{\text{f}} = -\kappa\varepsilon_{\text{f}}\mathrm{B}_{zz} \tag{A4}$$

$$\mathrm{K}_{\text{sf},\,zz}/k_{\text{f}} = \mathrm{K}_{\text{fs},\,zz}/k_{\text{f}} = -\kappa\varepsilon_{\text{f}}\mathrm{B}_{zz} \tag{A5}$$

$$\mathrm{K}_{\text{ss},\,zz}/k_{\text{f}} = \varepsilon_{\text{s}}\kappa\left(1+\kappa\frac{\varepsilon_{\text{f}}}{\varepsilon_{\text{s}}}\mathrm{B}_{zz}\right) \tag{A6}$$

Note that the following correlation holds:

$$\mathrm{K}_{\text{eff},\,zz} = \mathrm{K}_{\text{ff},\,zz} + \mathrm{K}_{\text{fs},\,zz} + \mathrm{K}_{\text{sf},\,zz} + \mathrm{K}_{\text{ss},\,zz}. \tag{A7}$$

As an example, considering case RR with $\varepsilon_{\text{f}} = 0.25$ and $\kappa = 1000$, the effective conductivity is $\mathrm{K}_{\text{eff}}/k_{\text{f}} = 577.6$. From Eq. (A2) $\mathrm{B}_{zz} = -6.900e-4$. The corresponding dimensionless conductivity components are

$$\mathrm{K}_{\text{ff},\,zz}/k_{\text{f}} = 0.25(1-6.900e-4) = 0.2498$$

$$\mathrm{K}_{\text{fs},\,zz}/k_{\text{f}} = \mathrm{K}_{\text{sf},\,zz}/k_{\text{f}} = 0.1725$$

$$\mathrm{K}_{\text{ss},\,zz}/k_{\text{f}} = 577.5$$

References

[1] R.G. Carbonell, S. Whitaker, Heat and mass transfer in porous media, in: J. Bear, M.Y. Corapcioglu (Eds.), Fundamentals of Transport Phenomena in Porous Media, Martinus Nijhoff, Dordrecht, The Netherlands, 1984, pp. 123–198.

[2] M. Quintard, S. Whitaker, One and two-equation models for transient diffusion processes in two-phase systems, Adv. Heat Transfer 23 (1993) 369–465.

[3] F. Zanotti, R.G. Carbonell, Development of transport equations for multiphase systems — III. Application to heat transfer in packed beds, Chem. Engng. Sci 39 (1984) 263–278.

[4] M. Quintard, S. Whitaker, Local thermal equilibrium for transient heat conduction: theory and comparison with numerical experiments, Int. J. Heat Mass Transfer 38 (1995) 2779–2796.

[5] G. Grangeot, M. Quintard, S. Whitaker, Heat transfer in packed beds: interpretation of experiments in terms of one- and two-equation models, in: Proceedings of the 10th International Heat Transfer Conference, Brighton, UK, vol. 5, 1994, pp. 291–296.

[6] M. Kaviany, Principles of Convective Heat Transfer, Springer-Verlag, New York, 1994 (Chap. 5).

[7] H.Y. Zhang, X.Y. Huang, C.Y. Liu, Studies of convection heat transfer in porous media characterized by straight ducts, in: Proceedings of the 5th ASME/JSME Thermal Engineering Joint Conference, 1999.

[8] S.V. Patankar, Numerical Heat Transfer and Fluid Flow, Hemisphere, New York, 1980.
[9] S.V. Patankar, C.H. Liu, E.M. Sparrow, Fully developed flow and heat transfer in ducts having streamwise-periodic variation of cross-sectional area, J. Heat Transfer 99 (1977) 180–186.
[10] I. Nozad, R.G. Carbonell, S. Whitaker, Heat conduction in multiphase systems — I. Experimental method and results for two-phase systems, Chem. Engng. Sci 40 (1985) 843–855.
[11] M. Sahraoui, M. Kaviany, Slip and no-slip temperature boundary conditions at interface of porous, plain media: conduction, Int. J. Heat Mass Transfer 36 (1993) 1019–1033.
[12] M. Sahraoui, M. Kaviany, Slip and no-slip temperature boundary conditions at the interface of porous media: convection, Int. J. Heat Mass Transfer 37 (1994) 1029–1044.
[13] W.M. Kays, M.E.C. Crawford, Convective Heat and Mass Transfer, 3rd ed., McGraw-Hill, New York, 1993 (Chap. 9).